AMERICAN JOURNALS
Open Access, Peer Reviewed Journals

American Journal of Technology and Applied Sciences
ISSN (E): 2832-1766 Volume 42, November - 2025

THE EFFECT OF 5 MeV ELECTRON IRRADIATION AT 165 K ON THE STRUCTURAL AND MAGNETIC PROPERTIES OF YBCO BASED HTSC TAPE

Mussaeva Malika Anvarovna,
Shodiev Akhmad Abdunabiyevich
Institute of Nuclear Physics of the Academy of Sciences of the Republic of Uzbekistan, Tash-kent, Uzbekistan,
E-mail: mussaeva@inp.uz, akhmadshodiyev@gmail.com

ABSTRACT

We investigated the impact of 5 MeV electron irradiation at 165 K (close to the superconduct-ing transition temperature Tc 90 K) on the structural transformations and charge transport at applied magnetic field 0.56 Tesla to YBa_2Cu_3O7-x (YBCO)-based and coated with Pb-Sn-Cu-Ag- layers high-temperature superconductor (HTSC) tapes of the second generation, which are already used in charge particle accelerators and magnetic plasma confinement systems. Meth-ods of XRD for structure-phase analysis revealed the irradiation induced recrystallization both in metal coatings and in YBCO-film, so the YBCO layer was exposed to mixed fluxes of elec-trons and bremsstrahlung gamma-quanta. Hall Effect measurements were implemented for de-termining electron and hole contributions in electric conductivity, magnetoresistance in the temperature range 80–320 K. Origin double-Y-plotting allowed to distinguish hole (peak at 160 K) and electron carriers and condensation from localization temperatures. Displacement de-fects responsible for the radiation induced transformations in YBCO crystallites are mainly in oxygen and copper sublattices. Interfaces YBCO-Y2O3 and YBCO-CuO serve as artificial pin-ning centers, generated both during chemical deposition and irradiation.

KEYWORDS

YBCO-film, electron irradiation, bremsstrahlung gamma-emission, Hall effects, recrystallization.

Introduction

Currently metal coated HTSC electric cables (wires or tapes) have such a high critical current density $J_c \sim 6$ kA in applied magnetic field 2 T at 30 K that are replacing magnetic coils in charge particle accelerators and magnetic plasma confinement systems [1–4]. Their advantages come from generation of artificial pinning centers (APC) in HTSC both by chemical and radiation treatments, which were studied experimentally. The demand for HTSC solenoids for thermal nuclear synthesis obviously assumes the radiation methods, therefore molecular dynamics simulations of radiation damage in

$YBa_2Cu_3O_7$ were done taking into account structure anisotropy and complexity [5]. Figure 1 demonstrates the best technological solution to deposit a micron layer of crystalline HTSC film (RE- stands for Yttrium or rare earth elements, BCO denotes Ba-Cu-Oxygen) by pulse laser deposition method (PLD) on a polished steel tape not directly, but preliminary coated with a few crystalline nanolayers with the lattice parameters approaching to those of HTSC [6]. Such a technology was the basis of Concept of the High-Temperature Superconductor Magnetic System of the New Nuclotron Synchrotron [7]. The complicate anisotropical structure of (RE)BCO introduces corresponding anisotropy of the tape: *ab*-plane of (RE)BCO along the length corresponds to azimuthal direction in a coil; *ab*-plane along the width corresponds to axial direction (z axis) in a coil; the c-axis direction, perpendicular to ab plane corresponds to radial direction in a coil [6].

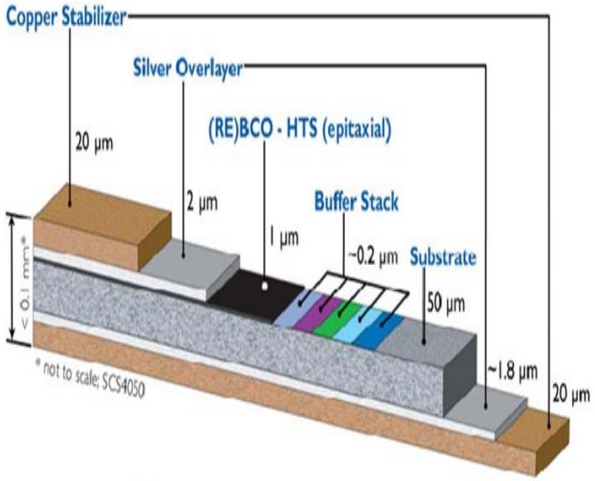

Fig. 1. Schematic design (not to scale) of the coated (RE)BCO microfilm deposited on the multilayer buffer stack deposited on the steel tape and coated with silver contact and copper stabilizer [6]

Figure 2 shows the detailed unit cell of YBCO and the result of molecular dynamic simulations of unstable and stable interstitial positions of atoms displaced by fast (>0.1 MeV) neutrons [5]; the authors found fractional charges of all cations and anions of YBCO: Y(+1.9), Ba(+1.5), Cu(+1.4), O(−1.3); the number of defects formed at the operational temperature of 25 K is predicted to be lower than observed at 360 K due to creation of more defects during the ballistic phase coupled with inefficient recombination during the annealing phase at the higher temperature.

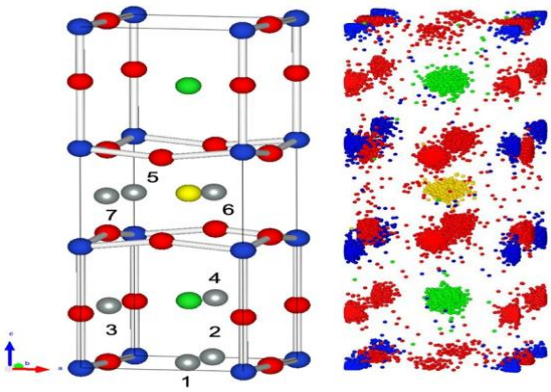

Fig. 2. Graphical representation of the $YBa_2Cu_3O_7$ unit cell. Red, blue, green and yellow spheres correspond to oxygen, copper, barium and yttrium, respectively: left- the grey spheres 1–7 illustrate possible interstitial sites for displaced atoms during the cascade; right – accumulated image of 3328 atoms in $YBa_2Cu_3O_7$ supercell folded down to its unit cell at 5.4 ps (toward the end of the recombination phase equilibrated at 25 K), the interstitial 1–2 sites have been populated with Oxygen interstitials (red) [5]

The study used DFT modeling of Cu K-edge defect structures and high-energy X-ray spectroscopy to gain new insights into the nature of defects induced by He^+ ion irradiation, and to find clear evidence of defects in copper planes in addition to XRD and TEM data [8]. The authors showed that Frenkel defects, consisting of oxygen vacancies at the in-plane O(2) site and oxygen vacancies between the Cu(2) and Cu(3) planes, are known to be relatively low-energy defects and reproduce many of the spectral and crystallographic changes observed after ion irradiation [8]. A decrease in the J_c was observed in a thin $YBa_2Cu_3O_{7-x}$ film after its irradiation with 4 MeV electrons at a dose of $3 \cdot 10^{16}$ electron/cm^2. The temperature dependence of J_c is consistent with the idea of a granular structure of the film with intercrystalline contacts of the superconductor-metal-insulator-superconductor type [9]. Later, the authors irradiated $YBa_2Cu_3O_{7-x}$ films with 1 MeV electrons and to a higher dose of $4 \cdot 10^{16}$ electron/cm^2 limited by the condition that defects formed as a result of electron-nuclear collisions cause an insignificant decrease in the critical temperature T_c. Under this condition, the main source of radiation effects can be the excitation process of the electron subsystem of $YBa_2Cu_3O_{7-x}$ [10]. When YBCO films were irradiated with electrons from 20 keV to 2.4 MeV at doses from 10^{18} to 10^{22} electron/cm^2, a continuous decrease in T_c was observed with increasing dose. This is in good agreement with estimates of the number of defects formed at such doses by the electron-nuclear collision mechanism [11]. Previously, we achieved an increase in the magnetization hysteresis (i.e., the current J_m) in fields of 3–4 Tesla in YBCO single crystals after irradiation with electrons with energies of 300 – 350 keV (sufficient to displace only the oxygen atoms responsible for pinning at 0.5 Tesla) and 1 MeV (sufficient to displace the copper atoms responsible for vortex pinning at 3 Tesla) at doses up to 10^{19} cm^{-2} with a decrease in T_c by only 2 K [12,13-]. However, these encouraging results in the case of modern HTSC tapes with metal coatings should be sought under other irradiation conditions, taking into account the inevitable energy losses during the penetration of metal layers covering the HTSC, the already discovered dose limits for reducing J_c and the need to maintain the HTSC phase with T_c~90 K. Then we studied the surface condition of HTS tapes (YBaCuO) exposed to 5 MeV electron fluency 10^{15} cm^{-2} at beam current density 1 μA/cm^2 in air at 273 K, suggesting significant energy losses at interaction with heavy upper microlayer of PbSn solder (the total ionization energy 1.85 MeV for Pb and 0.45 MeV Sn was calculated) and found that it has practically decomposed into Pb nanocrystallites (height 20–70 nm) over Sn nanofilm, then microtube Cu coated with a thin nanolayer CuO, and under it a crystalline microfilm of $YBa_2Cu_2O_7$, under which there is a thin crystalline layer of Y_2O_3 on the surface of the substrate steel tape [14].

The irradiation at low temperature generates new “shallow trap” states in the CuO_2 planes, into which oxygen migrates. When oxygen in the CuO chains becomes less stable, it transitions to the CuO_2 planes, reducing electron density and thus creating holes. These transitions promote hole doping. An increased hole concentration in the CuO_2 planes strengthens superconductivity, raising the critical temperature (T_c). At relatively low temperatures, atomic motion within the lattice slows, and diffusion

and recombination processes decelerate. The vacancies, interstitials, and oxygen dislocations resulting from electron irradiation do not consolidate quickly – in other words, the defects "freeze" and remain within the structure for extended periods. These defects may have a substantial impact on superconductivity, particularly by enhancing pinning centers, which in turn can increase the critical current density (J_c). Pinning stabilizes vortices in place, thereby increasing J_c. Irradiation suppresses vortex motion, reducing energy loss. When vortices move freely, they introduce resistance to superconductivity. If they are pinned, the material performs ideally. The structural defects caused by irradiation aid in vortex pinning, allowing the material to retain superconductivity even under high magnetic fields.

The aim of this work was to determine the irradiation conditions when a spatial defect density is much less and possible increases the critical current in multilayer HTSC-YBCO tapes.

Sample details & methods

Sample details. The study focused on 2G HTS wire fabricated using industrial equipment at the SuperOx group of companies – S-Innovations LLC (Moscow, Russia) and SuperOx Japan LLC (Kanagawa, Japan). The wire architecture consists of a cold-rolled Hastelloy C276 substrate, a biaxially textured MgO buffer layer deposited by ion beam assisted deposition (IBAD), and a $YBa_2Cu_3O_7$ HTS layer applied using pulsed laser deposition (PLD). The industrial YBCO tapes are 4 mm wide and engineered to operate under a magnetic field of 20 Tesla at 20 K. Their critical current at 77 K reaches 150 A. The YBCO crystal film is coated with micro-layers of Ag, Cu, and PbSn [2,-15].

Irradiation. The samples were cooled to 165 K and irradiated with 5 MeV electrons along the c-axis using the U003 electron accelerator at the Institute of Nuclear Physics, Academy of Sciences of the Republic of Uzbekistan. Irradiation was performed for 200 seconds at a fluence of 5Ч10№⁴ electron/cm2, with a beam-to-sample distance of 48 cm and an irradiation current of 400 nA. Cooling was achieved by transferring the temperature of liquid nitrogen through a specially designed copper support that held the samples. The dewar, filled with liquid nitrogen, accommodated the copper support such that one-fifth of its length (where the samples were mounted) remained exposed to air, while the rest was submerged in nitrogen. To prevent direct interaction between the electron beam and the liquid nitrogen during irradiation, the dewar was shielded with a metal cover of sufficient thickness.

The X-ray diffraction spectra of the nonirradiated and irradiated samples were taken on an XRD Empyrean X-ray diffractometer (PANalytical, Netherlands) in the wide range (2 Theta, 10°–130°) [16]. The phase composition was determined using the PDF-2016 and COD databases. The measured X-ray diffraction spectra of the SuperOx-1 tape, along with the FWHM and crystallite sizes, were calculated and plotted using OriginPro 2018 SR1 software. The XRD spectra were compared to those in [17]. The magnetic and electric characteristics were studied by the four-point probe Hall Effect method on the HMS-7000 system and the AMP55T magnet kit used for measurements at low temperatures (80–350 K) theoretical basis is Lorentz Force and Van der Pauw technique (Ecopia, South Korea). The sample tapes each 5 cm long were fixed with 4 gold-coated contacts on the stage. The measurements were taken at magnetic field of B=0.556 T directed normally to the tape surface and a current of I=10 mA.

Results and discussion

XRD measurements

Fig. 3a–d shows X-ray diffraction spectra of YBCO tape SuperOx-1 before and after electron irradiation at 165 K, taken in reflection mode on an X-ray diffractometer Empyrean at 300 K. In the non-irradiated sample, weak reflections and an increased low-angle background were detected from amorphous phases and intense reflections from crystalline phases.

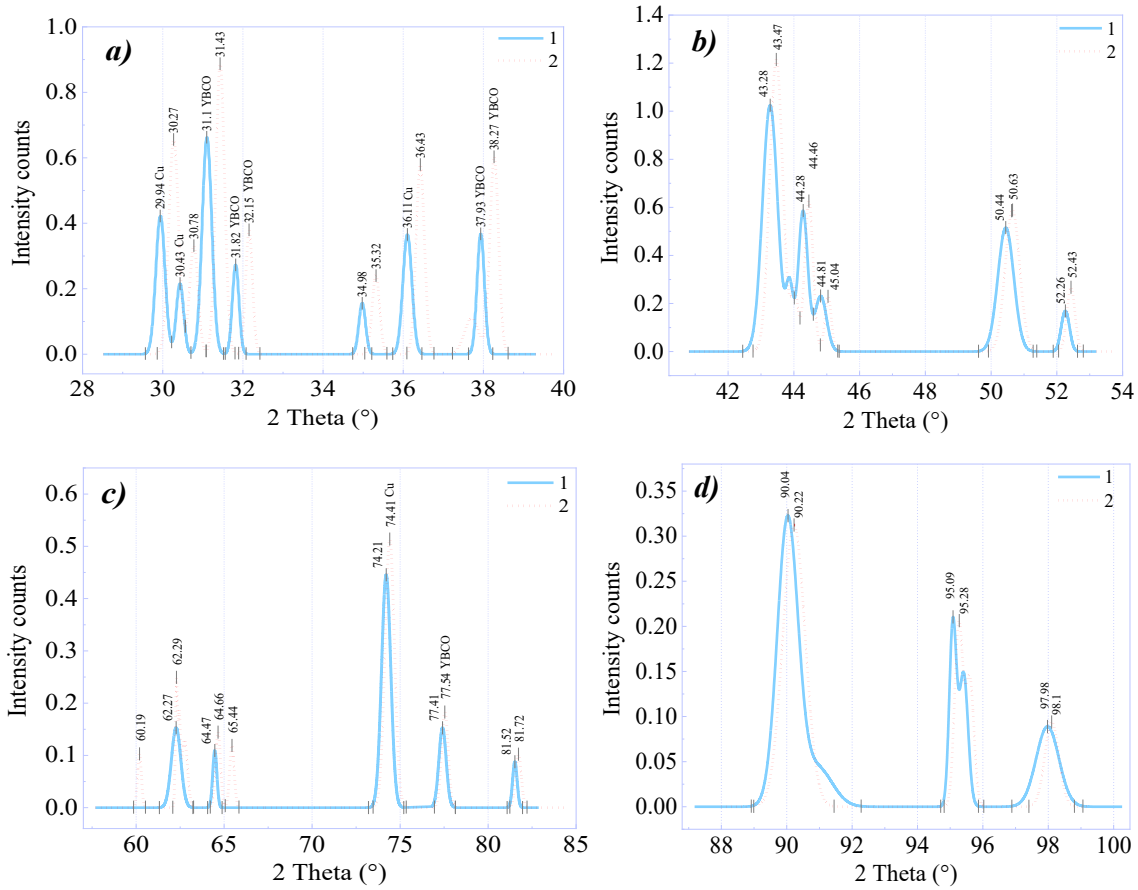

Fig. 3. The fragmental X-ray diffraction spectra of the SuperOx-1 tape, obtained using the XRD method, are represented by the corresponding intensity peaks in the X-ray diffraction spectra (*a*, *b*, *c*, and *d*), which are related to the 2θ angle. 1 – Reference, 2 – Irradiated integral fluency of 5Ч10^{14} electron/cm^2 at the energy of 5 MeV at 165 K

Figures 3 *a-d* illustrate that, following electron irradiation, the diffraction peak intensities increase and shift to the right along the x-axis – most noticeably in Figure 3a. Furthermore, the crystallite sizes at the corresponding angles (as shown in Figures 3 *a-d* and summarized in Table 1) are either reduced or increased after irradiation because of changing crystal orientation at interfaces. Crystal sizes D were calculated by the known formula:

$$D = \frac{K\lambda}{\beta \cos\theta} \qquad (1)$$

where:

D – crystallites size (nm) within the coherent scattering area;

K – 0.94 (Scherrer constant);
λ – 0.15406 nm (wavelength of the X-ray source);
β – FWHM Left [°2θ] (full width at half maximum);
θ – Peak position (Bragg angle).

Table 1. Structure and phase analysis and calculated crystallite size values of YBCO-tape: left- the reference, right- after electron irradiation to dose 5Ч10^{14} electron/cm^2 at 165 K

Reference				Irradiated			
2 Theta (°)	FWHM	Crystal size D (nm)	Phases	2 Theta (°)	FWHM	Crystal size D (nm)	Phases
29.9430	0.2705	31.75	Cu,Y_2O_3	30.2747	0.2922	29.41	Y_2O_3
30.4296	0.2149	40.02	Cu, PbSn	30.7719	0.2535	33.94	Sn, PbSn
31.1037	0.2823	30.51	YBCO, Cu, Pb	31.4337	0.2590	33.28	Pb
31.8195	0.1942	44.42	YBCO, Sn	32.1546	0.1990	43.39	YBCO,CuO, PbSn
34.9763	0.1965	44.27	CuO	35.3171	0.2187	39.81	CuO,
36.1039	0.2644	33.00	Cu, Pb	36.4246	0.2468	35.39	Y_2O_3
37.9338	0.2156	40.69	YBCO	38.2683	0.2277	38.56	Ag, YBCO
43.2797	0.5517	16.18	Cu	43.4691	0.4341	20.57	Cu
44.2771	0.2770	32.34	Ag	44.4549	0.2996	29.91	Ag, Y_2O_3,Sn
44.8024	0.4521	19.85	PbSn	45.0413	0.2260	39.73	PbSn
50.4475	0.5699	16.09	YBCO,Cu	50.6483	0.5185	17.70	Cu, YBCO
52.2587	0.2950	31.33	Cu	52.4267	0.2881	32.10	YBCO, Pb
62.2715	0.6238	15.54	Sn, Pb	62.4930	0.6718	14.44	PbSn, Pb, Sn
64.4695	0.2766	35.46	PbSn	64.6539	0.3045	32.24	Sn
74.2069	0.6110	17.03	PbSn	74.4102	0.6290	16.56	CuO, Cu
77.4090	0.4837	21.98	Ag	77.5424	0.4396	24.20	YBCO, Ag
81.5191	0.3006	36.44	CuO	81.7201	0.3797	28.89	Ag,
90.0533	0.7754	15.14	Cu	90.2218	0.8067	14.57	Cu
95.2183	0.5658	21.75	YBCO	95.3833	0.5741	21.47	YBCO, PbSn
97.9780	0.8149	15.52	CuO	98.1080	0.5043	25.11	CuO

The table shows that in this multilayered system there are at least 5 different interfaces of different crystalline compounds, which are contacted with planes having very close interatomic distance d responsible for one common reflection. After the intensive irradiation we see changes in the reflection angles and contacting phases. It means recrystallization of phases at interfaces with their reorientation towards to the best interatomic distance matching. Either increase or decrease of crystallite size indicates fragmentation, while increased size suggests grain growth or recrystallization under irradiation. One should take into account, the irradiation induced recrystallization both in metal coatings and in YBCO-film, so the YBCO layer was exposed to mixed fluxes of electrons and bremsstrahlung gamma-quanta.

Hall effect measurements

Before presenting our Hall effect measurements in applied magnetic field 0.5 T, a brief review is done below on generation of point defects by electron and gamma-quanta, which act as point pinning centers for flux vortices increasing the critical current density J_c in superconducting YBCO. Unlike 1–4 MeV electron irradiations capable of displacing any atom of YBCO [9–11], low energy 30 keV electron

irradiation below and above 10^{20} electron/cm^2 of YBCO thin films (75–200 nm) resulted in increase and decrease in the J_c, which are controlled by changes in the density of oxygen vacancies acting as effective pinning centers. The Raman investigations suggest that critical temperature increase in irradiated films is due to healing of broken CuO chains that results in increased carrier's concentration in superconducting CuO_2 planes [18] .

Like electron irradiation, gamma radiation also significantly influences the electrical and magnetic properties of YBCO tapes by effect over the oxygen random distribution on the basis plane, specially over the Cu(1)-O chain sites, the electronic movement of the Cooper pairs ascribed to the YBCO superconducting properties takes place at the Cu(2)-O_2 planes. Gamma radiation with initial energies $E_\gamma \geq 129$ keV can displace Oxygen and $E_\gamma \geq 489$ keV displace Copper, as well, in the Cu(2)-O_2 planes [19]. Also, the electrical resistivity in the normal state shows a nearly linear dependence on the exposure dose, which is expected to be due to the increase in vacancy concentration in the Cu(2)-O_2 planes upon gamma irradiation, based on Mathiessen's rule. In relation to the superconducting transport properties, gamma irradiation has been shown to enhance the vortex pin energy U_0 and the critical electric current J_c in superconducting state [20]. To refer to theoretical work, as expected for a single-band metal with a hole density n =1+p, while the overdoped metallic state is characterized by a single large hole Fermi surface whose volume contains 1+p holes per Cu atom, as determined by angle-dependent magneto resistance (ADMR) [21]. The normal-state Hall effect and magnetoresistance of single crystals of $Tl_2Ba_2CuO_{6+\delta}$ with $T_c < 15$ K was studied in the elastic-scattering regime up to 30 K The temperature dependence of the Hall coefficient, R_H, below 30 K rules out models in which R_H(T) is taken as a measure of a real temperature-dependent change in the carrier concentration. The two scattering rates (probed by the resistivity and the cotangent of the Hall angle) which characterize normal-state transport in the cuprates $T \geq 30$ K [22]. The electrical resistivity ρ(T) exhibits the standard T^2 temperature dependence of a Fermi liquid [23]. At intermediate doping, between the insulator and the metal, there is a central region of superconductivity, delineated by a critical temperature T_c which can rise to values of order 100 K. Above the maximal T_c, near optimal doping, the normal state is a “strange metal”, characterized by a resistivity which is linear in temperature instead of quadratic. In the midst of this strange-metal region, the enigmatic “pseudogap phase” sets in, below a crossover temperature T* where most physical properties undergo a smooth yet significant change [24]. In a model of charge carriers on a three-dimensional Fermi surface scattered by two-dimensional antiferromagnetic spin fluctuations, transport properties near the magnetic quantum critical point are found to be dominated by “hot spots”, points on the Fermi surface connected by the ordering wavevector. In this case, calculations show that ρ(T) ~ T, $C_e/T \sim \log(1/T)$ and $S/T \sim \log(1/T)$ [25]. More generally, both ρ(T) ~ T and $C_e/T \sim \log(1/T)$ follow naturally from a marginal Fermi liquid phenomenology [26]. The low frequency of quantum oscillations and the decrease in Hall coefficient to deeply negative values below 100 K observed in YBCO near p = 1/8 demonstrate that the large hole Fermi surface of overdoped cuprates undergoes a profound reconstruction in the pseudogap phase. However, the lack of evidence for static stripe order in YBCO at p = 1/8 raises interesting questions: are fluctuating charge/spin modulations sufficient to alter the Fermi surface , and where the pseudogap phase is a fluctuating precursor of a long-range stripe order that only sets at lower temperatures than T* [27], [28], [29]. The effect of electron irradiation below the energy threshold for the formation of in-plane defects on the resistance, and Hall coefficient in thin $YBa_2Cu_3O_{7-x}$ films fully doped with

oxygen was studied. It was shown that the observed changes can be explained by the disruption of the oxygen chain (the formation of vacancies at the O(1) and O(5) positions), which, firstly, disrupts the conductivity of the chains, and secondly, reduces the hole doping in the CuO_2 planes [30]. The results of this work allow the authors to conclude that the T-line resistance slope and the increase in the Hall coefficient of YBCO observed in many irradiation experiments with high-energy particles [31, 32] are also due to the formation of defects in the chains, which occurs simultaneously with the formation of in-plane defects. However, the T~ suppression is primarily due to in-plane defects [30]. The particular attention was paid on the individual (isolated) damage cascade production by irradiation with 50 keV Kr^+ and 89 keV Xe^+ ions to low fluencies $(1–4)\times10^{11}$ cm^{-2} of YBCO crystals in the superconducting state at 40 K well below the T_c=91 K, followed by TEM analysis at 40 K and after annealing to 100 K, 170 K, 240 K and finally to 300 K under focused 100 keV electron beam (*in-situ*) [33]. The authors distinguished the vacancy and interstitial types of strain fields and observed non-coherent recrystallization within 20 unit cells (8 nm) involving rotation of *a*-*b*-*c*-axes. To imitate the operation condition of HTSC accelerators at the electron energy of 2.5 MeV at 10 K, YBCO single crystals were irradiated at the beam angle 5° to *c*-axis to high doses $(1–3)\times10^{18}$ cm^{-2} at the dose rate 4.2×10^{13} $cm^{-2}sec^{-1}$. Magnetization current was measured at applied field 1 kOe, 10^{-6} V/cm, 85 K just below the T_c. The authors estimated the vortex size a=140 nm and the distance between twins 300 nm as optimal electron irradiation condition [34]. Figure 4 provides schematic illustration of the charge-transfer between chains and planes, taking place when YBCO is cooled through the metal-superconductor transition (MST), and the relevant orbitals for the self doping mechanism, which are the (partially empty) and orbitals at the chain Cu(1) and plane Cu(2,3)-sites and the connecting apical oxygen O(4) orbitals [35].

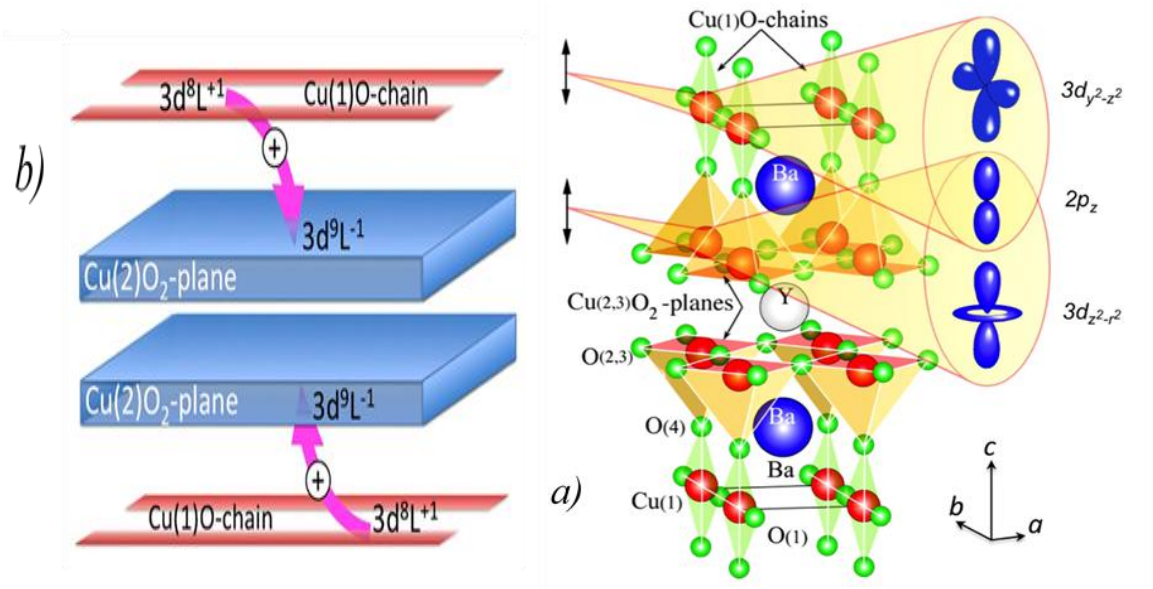

Fig.4. (a) Schematic illustration of the charge-transfer between chains and planes, taking place when YBCO is cooled through the MST. In the superconducting phase the $3d^8L^{+1}$ configuration at Cu(1)-sites in the chains is suppressed, while at Cu(2)-sites the $3d^9L^{-1}$ configuration is increased. The net effect is a self doping of the superconducting planes in the MST. (b) The relevant orbitals for the self doping mechanism are the (partially empty) $3d_{z^2-r^2}$ and $3d_{y^2-z^2}$ orbitals at the Cu(1) and Cu(2,3)-sites

and the connecting apical oxygen O $2p_z$ orbitals. The first ones are preferentially excited when aligning the *x*-ray polarization vector along the c-direction (out of-plane) [35]

Concluding from the above review, irradiation of modern metal coated superconductor micro sized tape with high-energy electrons >4 MeV at moderate beam current (dose rate <μA/cm^2) to quite low doses so as to generate well separated defect cascades as magnetic pinning places at low temperatures makes it possible to create HTSC coil for charged particles accelerators. One may expect radiation defects in recrystallized places. These defects would change the electrical resistance in both normal (above T_c) and superconducting (below T_c) states.

Figures 5 (*a*, *b*, *c*, *d*, *e*) show our results of Hall effect measurements prior and after 5 MeV electron irradiation at 165 K to fluency 5Ч10^{14} electron/cm^2 at the electron beam current density 400 nA/cm^2, including temperature dependencies of resistivity ρ (*a*), magnetoresistance R in the applied magnetic field 0/56 Tesla directed normal to both voltage and current (*b*), carrier mobility μ (*c*), Hall coefficient R_H (*d*), bulk carrier concentration n *(e*).

Before describing the ρ(T) and discussing the conductivity mechanism, we should emphasis that both voltage and current signals go between the four golden contacts in the Hall cell through PbSn-Cu-Ag microlayers towards YBCO microfilm and back as shown in Table 1.

It is known that the most effective charge scattering or trapping takes place at the interfaces of various metals having different conductivity.

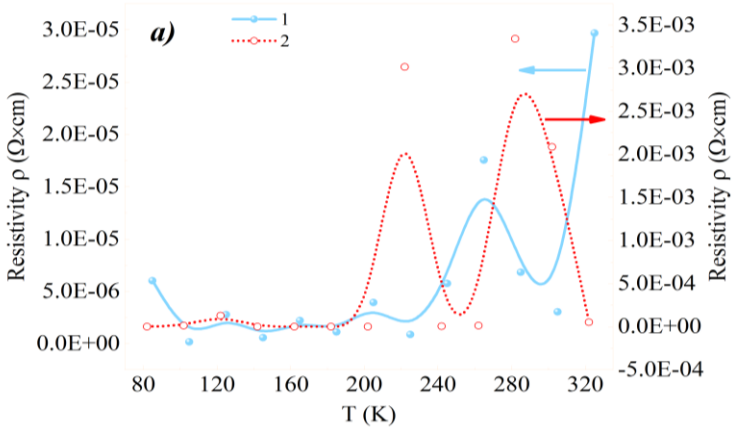

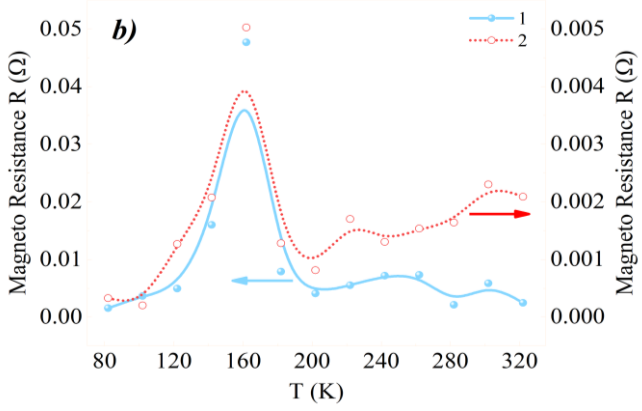

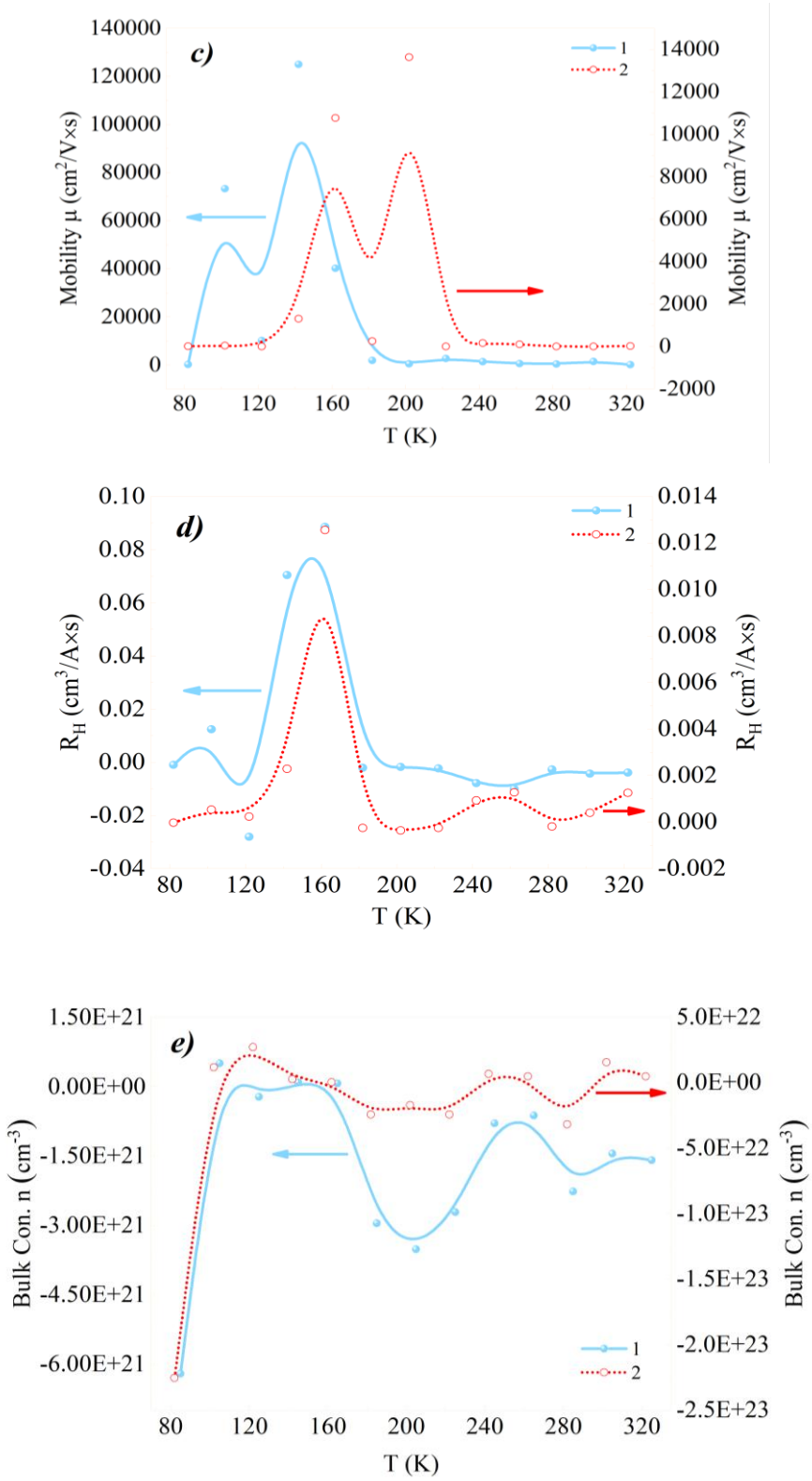

Fig. 5. Resistivity ρ (*a*), Magnetoresistance R (*b*), Carrier mobility μ (*c*), Hall coefficient R_H (*d*), Bulk concentration n (cm^3) 1 – reference, 2 – after irradiation at 165 K with the fluency of 5 MeV electrons 5Ч10^{14} electron/cm^2

Fig 5*a* shows a "strange" metal behavior nearly constant resistivity within 100–230 K, followed by the normal metal T^2 range with peaks at 270 K and > 320 K, where charge carriers are localized. After the electron irradiation the resistivity increased resistivity by a factor of 20 because of formation of two traps at 220 and 290 K. Fig.5*b* demonstrates a strong (in applied magnetic field 0.56 Tesla) magnetoresistance band peaked at 160 K, which 10 times decreases after the irradiation. According to the finding [5] the most stable defects in oxygen sublattice are oxygen interstitials in O(5) sites, which trap holes, and the residual oxygen vacancies O(1), which trap electrons. The both are responsible for the paramagnetic peaks at 160 K (non-irradiated) and weaker ones at 120, 230 and 290 K. To distinguish electron and hole traps only by the carrier mass, the mobility was measured as shown in fig. 5*c*. Abrupt mobility drop below 100 K should be attributed to charge carrier condensation into HTSC state. Indeed, 10 times higher electron mobility peaked at 140 K may be due to the magnetic vortex state. After the irradiation the mobility decreases 10 times and the maximum shifts towards 160 and 200 K. Such behavior correlates with domination of hole trapping oxygen centers in Y_2O_3 and the related complicate compounds [12, 13]. The mobility decrease above 140 K in non-irradiated sample and above 200 K may be explained by thermal activation of magnetic vortices around hole trapping centers, according to [35]. Comparing fig. 5*b* and fig. 5*d* one can see their similarity and conclude that magnetic resistance peak at 160 K to hole carriers. However after the electron irradiation there added some contribution from generated electrons. Despite the irradiation induced defects the bulk carrier concentration (Figure 5*e*) increased by approximately 10 to 20 times and stabilized at the level of 10^{22} cm^{-3} above the superconductivity onset temperature below 120 K. The conductivity, dominates by hole transfer from CuO chains to CuO_2 plane according to the charge transfer scheme [35] and the estimated effective fractional valence of $Cu^{1.4+}$ and $O^{1.3-}$ [5]. Based on the above observations, it can be concluded that 5 MeV electrons induce defects in the superconducting YBCO layer of HTS tapes when irradiated at relatively low temperatures, namely 165 K. These defects appear to remain well preserved, especially when the irradiated sample is kept at liquid nitrogen temperature for several hours immediately after irradiation.

Conclusion

Comparing XRD phase analysis of HTSC with chemical pinning centers (non-superconducting oxide on the YBCO surface) and the irradiation induced centers (recrystallized oxide-metal-YBCO) are functionally similar each to other. Mixed magnetic vortex state occurs in the temperature interval 100–300 K depending on the radiation induced defects. Methods of XRD for structure-phase analysis revealed the irradiation induced recrystallization both in metal coatings and in YBCO-film, so the YBCO layer was exposed to mixed fluxes of electrons and bremsstrahlung gamma-quanta. In order to determine whether the induced defects are stable or unstable, measurements must also be conducted after a certain delay following irradiation. In real situation measurements of XRD and Hall effect were done in different time after the irradiations, therefore the irradiated samples were in various temporal relaxation states. In our previous studies, we remeasured room-temperature irradiated samples one year later and found that only a small fraction of the initial results were reproducible. Therefore, remeasuring samples irradiated at 165 K after a controlled delay may yield highly interesting and important data for future investigations. But in the practical application as the HTSC based accelerator

or tokamak, the operation (irradiation) periods and the rest (relaxation) periods may be different, so the part of the irradiation induced defects will anneal during the rest period.

Controlled 5 MeV electron irradiation to 100 times less fluency and at lower temperature (165 K) than in optimized YBCO tape performance by enhancing the critical current. Radiation-induced defects act as effective pinning centers, stabilizing vortices under magnetic field 0.56 Tesla. Our method of electron irradiation seems promising for applications in high-field magnets and power cables.

Acknowledgement

The authors are grateful to Dr. S.I. Tyutyunnikov and PhD M.S. Novikov from the Joint Institute for Nuclear Research, Dubna, Russian Federation, for providing the samples and supporting the research. They also thank the INP AS RUz researcher prof. E.M. Ibragimova, PhD I. Yuldosheva for the XRD analysis and S. Egamov for measuring the Hall effect.

The researches are supported by basic funding allocated to the Institute of Nuclear Physics of the Academy of Sciences of the Republic of Uzbekistan by the decree PP-4526.

References

1. Fetisov S., Zubko V., Zanegin, S., Nosov A., Vysotsky V. Review of the design, production and tests of compact AC HTS power cables // Progress in Superconductivity and Cryogenics 22(4), 33–41 (2020).
2. Molodyk A., Samoilenkov S., Markelov A., Degtyarenko P., Lee S., Petrykin V., Gaifullin M., Mankevich A., Vavilov A., Sorbom B., Cheng J., Garberg S., Kesler L., Hartwig Z., Gavrilkin, S., Tsvetkov A., Okada T., Awaji S., Abraimov D., Francis A., Bradford G., Larbalestier D., Senatore C., Bonura M., Pantoja A. E., Wimbush S. C., Strickland N. M. & Vasiliev, A. Development and large volume production of extremely high current density $YBa_2Cu_3O_7$ superconducting wires for fusion //Scientific Reports 11, 2084 (2021). https://doi.org/10.1038/s41598-021-81559-z.
3. Khvostenko P.P., Anashkin I.O., Bondarchuk E.N., Inyutin N.V., Krylov V.A., Levin I.V., Mineev A.B., Sokolov M.M. Experimental thermonuclear installation tokamak T-15MD // Problems of Atomic Science and Technology, Ser. Thermonuclear Fusion 42(1), 15–38 (2019).
4. Meschini S., Laviano F., Ledda F., Pettinari D., Testoni R., Torsello D., Panella B. Review of commercial nuclear fusion projects // Frontier Energy Research. 11, 1157394 (2023).
5. Gray R.L., Rushton M.J.D., Murphy S.T. Molecular dynamics simulations of radiation damage in $YBa_2Cu_3O_7$ // Superconductor Science and Technology 35(3), 035010 (2022). https://doi.org/10.1088/1361-6668/ac47dc.
6. Song H., Brownsey P., Zhang Y., Waterman J., Fukushima T., Hazelton, D. 2G HTS coil technology development at SuperPower // IEEE Trans Appl. Supercond. 23(3), 4600806 (2013). doi: 10.1109/TASC.2012.2233837
7. Khodzhibagiyan H.G., Novikov M.S., Fisher E.Z., Shemchuk A.V. Concept of the High-Temperature Superconductor Magnetic System of the New Nuclotron Synchrotron // Physics of Particles and Nuclei Letters 21(1), 68–72 (2024). DOI: 10.1134/S1547477124010060.
8. Nicholls R.J., Diaz-Moreno S., Iliffe W., Linden Y., Mousavi T., Aramini M., Danaie M., Grovenor C.R.M., Speller S.C. Radiation-induced defects in high-temperature superconductors studied by high-energy X-ray spectroscopy // Communications Materials 3, 52 (2022).

9. Fedotov Yu.V., Ryabchenko S.M., Shakhov A.P. Critical currents in $YBa_2Cu_3O_{7-x}$ high-temperature superconducting thin films irradiated by 4-MeV electrons // Low Temperature Physics 26(7) 464–466 (2000). http:// dx.doi.org/10.1063/1.1306399.
10. Fedotov Yu.V., Danilchenko B.A., Rogutskii I.S. Low-dose radiation effects in thin films of high-temperature superconducting $YBa_2Cu_3O_{7-x}$ irradiated by 1-MeV electrons // Low Temperature Physics 28(10) 739–742 (2002).
11. Jackson E.M., Weaver B.D., Summers G.P., Shapiro P., Burke E.A. Radiation-induced T_c reduction and pair breaking in high-T_c superconductors // Phys. Rev. Lett. 74(15), 3033–3036 (1995). doi:10.1103/PhysRevLett. 74.3033.
12. Ibragimova E.M., Gasanov E.M., Nebesny A.F., Giapinzakis J. K., Kirk M. A. Oxygen defects in YBaCuO crystals after 300 keV electron and gamma-irradiations // Mater. Res. Soc. Proc. 540, 3291-8 (1999).
13. Ibragimova E.M., Kirk M.A. Modification of structure and properties of superconducting YBaCuO crystals by combined irradiation // Proc. Mater. Res. Soc. Symp. 659(II7) 8–13 (2001).
14. Shodiev A.A. The effect of 5 MeV electron radiation on the surface condition of HTS tapes (YBaCuO) / Republican scientific and practical conference on “Current problems of condensed matter physics and new high technologies” pp.135-137. Samarkand (2024).
15. Ibragimova E.M., Shodiev A.A., Ahrorova S., Mussaeva M.A., Iskandarov N.E., Kurbanov U.T. & Tashmetov, M.Yu. Low-dimensional magnetic centers in HTSC-YBCO film on steel-276 induced by gamma-quanta and electron beam // Journal of Magnetism and Magnetic Materials 595(171617), (2024). https://doi.org/10.1016/j.jmmm.2023.171617.
16. Shodiev A.A., Ibragimova E.M., Musayeva M.A., Iskandarov N.E., Baranov O.O., Tursunbaev I.Z. The effect of fast neutron irradiation on critical current of HTS tapes with nanoparticles // Center for advanced technologies International scientific conference of young scientists «Science and innovation» collection of scientific papers. pp. 346–348. Tashkent (2024).
17. Prabhakar B. and Wani T.A. "Crystal structure visualization and powder diffraction pattern of YBCO superconductor," /AIP Conference Proceedings. 2281 (020003), 1–6. (2020) doi: 10.1063/5.0026282.
18. Chromik S., Camerlingo C., Sojkovб M., Strbнk V., Talacko M., Malka I., Bar I., Bareli G., Jung G. Low energy electron beam processing of YBCO thin films // Applied Surface Science 389, 0169–4332 (2016).
19. Leyva A., Mora M., Martin G. & Martinez, A. Irradiation effect of ^{60}Co gamma rays in YBCO thick films // Supercond. Sci. Technol. 8(11), 816–821 (1995).
20. Leyva A. et al. The effects of ^{137}Cs and ^{60}Co γ- radiation on the magnetic susceptibility of BSCCO textured thin rods // Nucl. Instr. and Meth. B 239(3), 281–285 (2005).
21. Hussey N.E., Abdel-Jawad M., Carrington A., Mackenzie A. P., & Balicas L. A coherent three-dimensional Fermi surface in a high-transition-temperature superconductor // Nature, 425(6960), 814–817. (2003). https://doi.org/10.1038/nature01981.
22. Mackenzie A. P., Julian S. R., Sinclair D. C., & Lin C. T. Normal-state magnetotransport in superconducting $Tl_2Ba_2CuO_{6+\delta}$ to millikelvin temperatures // Physical Review B, 53(9), 5848–5855. (1996). https://doi.org/10.1103/PhysRevB.53.5848

23. Nakamae S., Behnia K., Mangkorntong N., Nohara M., Takagi H., Yates S. J.C., & Hussey N. E. Electronic ground state of heavily overdoped nonsuperconducting $La_{1.7}Sr_{0.3}CuO_4$ // Physical Review B, 68(10), 100502(R). (2003). https://doi.org/10.1103/PhysRevB.68.100502.
24. Timusk T., & Statt B. The pseudogap in high-temperature superconductors: An experimental survey // Reports on Progress in Physics, 62(1), 61–122. (1999). https://doi.org/10.1088/0034-4885/62/1/002.
25. Paul I., & Kotliar G. Thermoelectric behavior near the magnetic quantum critical point // Physical Review B, 64(18), 184414. (2001). https://doi.org/10.1103/PhysRevB.64.184414.
26. Varma C.M., Littlewood P. B., Schmitt-Rink S., Abrahams E., & Ruckenstein A.E. Phenomenology of the normal state of Cu-O high-temperature superconductors // Physical Review Letters, 63(18), 1996–1999. (1989). https://doi.org/10.1103/PhysRevLett.63.1996.
27. Kivelson S.A., Bindloss I.P., Fradkin E., Oganesyan V., Tranquada J.M., Kapitulnik A., & Howald C. How to detect fluctuating stripes in the high-temperature superconductors // Reviews of Modern Physics, 75(4), 1201–1241. (2003).
28. Kivelson S. A., Fradkin E., & Emery V. J. Electronic liquid-crystal phases of a doped Mott insulator // Nature, 393(6685), 551–554. (1998).
29. Hinkov V., Haug D., Fauque B., Bourges P., Sidis Y., Ivanov A., Chen C., Bernhard L., & Keimer B. Nernst effect in the pseudogap state of high-T_c superconductors // Science, 319(5863), 597–600. (2008).
30. Tolpygo S.K., Lin J-Y., Gurvitch M., Hou S.Y., Phillips J.M. T_c enhancement by low energy electron irradiation and the influence of chain disorder on resistivity and Hall coefficient in $YBa_2Cu_3O_7$ thin films // Physica C 269, 207–219 (1996).
31. Gupta R.P., & Gupta M. Effect of radiation-induced oxygen disorder on the superconducting transition temperature in YBCO superconductors // Physical Review B, 45(18), 9958. (1992).
32. Tolpygo S.K., Lin J.-Y., Gurvitch M., Hou S.Y., & Phillips J.M. Effect of oxygen defects on transport properties and T_c of $YBa_2Cu_3O_{6+x}$: Displacement energy for plane and chain oxygen and implications for irradiation-induced resistivity and T_c suppression // Physical Review B, 53(18), 12462. (1996).
33. Frishherz M.C., Kirk M.A., Zhang G.P., Weber, H.W. Transmission electron microscopy of defect cascades in $YBa_2Cu_3O_{7-\delta}$ produced by ion irradiation // Philos. Mag. A. 67, 1347–1363. (1993).
34. Bondarenko A.V., Prodan A.A., Petrusenko Y.T., Borisenko V.N., Dworschak F., Dedek U. Effect of electron irradiation on vortex dynamics in $YBa_2Cu_3O_{7-\delta}$ single crystals // Phys. Rev. B 64, 092513, (2001).
35. Magnuson M., Schmitt T., Strocov V.N., Schlappa J., Kalabukhov A.S., Duda L.-C. Self-doping processes between planes and chains in the metal-to-superconductor transition of $YBa_2Cu_3O_{6.9}$ // Scientific reports. 4, 7017, (2014). DOI: 10.1038/srep07017.